Sustain. Environ. Res., 21(1), 45-51 (2011)
(Formerly, J. Environ. Eng. Manage.)

PHOTOCATALYTIC DEGRADATION AND MINERALIZATION OF GASEOUS ISOPROPANOL OVER SILVER VANADATES

Chao-Ming Huang,[1,*] Lin-Shiang Huang,[1] Yi-Shan Li,[1] I-Hung Liu[2] and Ching-Yuan Chang[3]

[1]Department of Environmental Engineering
Kun Shan University
Tainan 710, Taiwan
[2]Green Energy & Environment Research Labs
Industrial Technology Research Institute
Hsinchu 310, Taiwan
[3]Graduate Institute of Environmental Engineering
National Taiwan University
Taipei 106, Taiwan

Key Words: Ag_3VO_4, visible-light driven photocatalyst, hydrothermal method

ABSTRACT

Visible-light-driven silver vanadate photocatalysts were synthesized using hydrothermal synthesis method. The structures of silver vanadates can be tuned by simply adjusting the hydrothermal time and adding the cetyltrimethylammonium bromide (CTAB). It is found that CTAB during the hydrothermal synthesis significantly affects the crystal structure, optical absorbance, and photocatalytic properties of silver vanadates. The pure silver vanadate oxides (SVO) consisted of mixed structures of $Ag_4V_2O_7$ and α-Ag_3VO_4, with α-Ag_3VO_4 as the major phase. For the CTAB-added sample, the α-Ag_3VO_4 phase was disappeared and the crystal phase of CTAB-SVO sample approached $Ag_4V_2O_7$. UV-Vis spectroscopy indicated that silver vanadate particles had strong visible light absorption with associated band gaps in the range of 2.2-2.4 eV. The sample prepared at 140 °C for 4 h (HT4) exhibits the best photocatalytic activity using the apparent rate constant for initial photodegradation of gaseous isopropanol and the mineralization yield after long term light irradiation. The enhancement of photocatalytic activity up to 3 times was obtained using HT4 with respect to the P25 (commercial TiO_2 photocatalyst). Surface characterization by Diffuse Reflectance Infrared Fourier Transform Spectroscopy confirms the presence of surface hydroxyl groups. The high activity can be attributed to the synergetic effects of strong visible-light absorption, favorable crystalline phase, and large surface hydroxyl groups.

INTRODUCTION

During the past decades, TiO_2 photocatalyst has been studied extensively for the photodegradation of pollutants and photocatalytic splitting of water under UV irradiation [1-3]. Numerous attempts have been made to develop the visible-light-driven photocatalysts to effectively utilize the solar energy due to the reason that visible light accounts for the largest proportion of the solar spectrum [4,5]. Until now, the visible-light-driven photocatalysts can be prepared by doping the metal or nonmetal elements to intercalate the donor levels in the forbidden band of TiO_2 [6]; or by exploring the new non-TiO_2-based semiconductor photocatalysts with valence bands consisting of hybrid orbitals of metal elements to reduce their band gaps. Recently, many ternary oxide photocatalysts such as $BiVO_4$, Bi_2WO_6, $AgNbO_3$ and Ag_3VO_4 were prepared by precipitation and solid-state reactions, and they were proven to be photoactive for water splitting under visible light irradiation [7]. Konta et al. [8] prepared silver vanadates (α-$AgVO_3$, β-$AgVO_3$, $Ag_4V_2O_7$ and Ag_3VO_4) by precipitation and solid-state reactions. They found that α-Ag_3VO_4 showed stronger photocatalytic activity than those of β-$AgVO_3$ and $Ag_4V_2O_7$ for O_2 evolution from an aqueous silver nitrate solution under visible-light irradiation. However, there has been very little research on the performances of α-Ag_3VO_4 and $Ag_4V_2O_7$ in the photodegradation of pollutants under visible-light illumination. The prepara-

*Corresponding author
Email: charming@mail.ksu.edu.tw

tion of the photocatalyst by solid-state reaction requires high-temperature and harsh fabrication conditions, mechanically mixed and reacted at 850 °C (or higher) for at least 12 h, with the outcome of larger, irregular particles, and small specific surface area. As a consequence, a lower photodegradation capability was expected [9,10]. To reduce energy consumption, exploiting low cost metal oxide catalysts with high visible-light photocatalytic activity is desirable.

It has been reported that the surfactant-assisted hydrothermal synthesis method can be as a relatively simple and high yield process to grow various metal oxides, such as TiO_2 [11], ZnO [12] and $BiVO_4$ [13], at much lower temperature (less than 200 °C), leading to the reduction of energy consumption. Isopropanol (IPA) is one of the main volatile organic compound emissions from waste gases in semiconductor manufacturing plants and is dangerous to human health [14]; IPA thus is chosen as the model pollutant to evaluate the visible-light photocatalytic activities of the as-prepared powders. The reaction mechanism of the photodecomposition of IPA by the catalysts was discussed using Diffuse Reflectance Infrared Fourier Transform Spectroscopy (DRIFTS) and Mass Spectrometry (MS) system. Surface characterization combined with activity tests can provide insight into the effects of hydrothermal time and surfactant on the phase formation and subsequently on the roles of surface hydroxyl groups in the reaction.

EXPERIMENTAL METERIALS AND METHODS

1. Catalysts Preparation

It has reported that the structure-directing agent and hydrothermal time play important roles in the fabrication of novel photocatalysts with various morphology and crystalline properties [15,16]. In the present study, three samples were synthesized by changing the hydrothermal time and with the assistance of a surfactant to obtain various crystal phases of silver vanadates. In a typical procedure to make the sample with molar ratio of Ag^+ to VO^{3-} equal to 3, 60 mL of 0.1 M $AgNO_3$ aqueous solution was added drop wise to 20 mL of 0.1 M NH_4VO_3 aqueous solution with a constant stirring. A suspended mixture was instantly formed and the pH value of the mixture was then adjusted to 7 with ammonia solution. After being aged for 24 h, the mixture was poured into a 100 mL Teflon-lined stainless reactor and heated to 140 °C for different hydrothermal treatment times in an oil bath. These samples were denoted as HT4 and HT6, indicating the hydrothermal treatment times of 4 and 6 h, respectively. The cetyltrimethylammonium bromide (CTAB)-silver vanadate oxides (SVO) samples were prepared by the addition of CTAB ($C_{19}H_{49}BrN$) with hydrothermal treatment of 4 h. After cooling to room temperature, the obtained brick red slurry was filtered and rinsed with distilled water to remove the NO_3^- and NH_4^+ residues. After the rinse, the samples were dried at 110 °C for 6 h.

2. Sample Characterization

The X-ray diffraction (XRD) patterns of the powders were measured using an X-ray diffractometer (Panalytical X'Pert PRO, Westborough, MA) with Cu radiation (λ = 0.15418 nm) in the 2θ-range from 10-60°. Infrared spectra of the surface hydroxyl group of the catalyst surface were collected using a DRIFTS system with an FTIR (Fourier Transform Infrared) spectrophotometer (PerkinElmer, spectrum GX, Shelton, CT). The DRIFTS system included a praying mantis diffuse reflectance accessory (Harrick Scientific, DRP-PE9, Pleasantville, NY), a controlled high temperature and low pressure reaction cell (Harrick Scientific, HVC-DRP-3, Pleasantville, NY), and an automatic temperature controller (ATC-024-1, Pleasantville, NY). Before DRIFTS measurements, the samples were pre-heated to 250 °C to remove adsorbed water. The pre-treatment process was set as follows: the samples were heated under vacuum and N_2 flow (30 mL min^{-1}) was introduced simultaneously, from room temperature to 250 °C, held at 250 °C for 30 min, and then cooled to 30 °C. DRIFT spectra were collected in the range of 2600-4000 cm^{-1} for surface hydroxyl groups. The measurements were converted to the Kubelka-Munk mode and some of the selected IR peaks were deconvoluted into several Gaussian curves to obtain the peak area information [17]. UV-Vis spectra were collected by a spectrophotometer (JASCO V-500, Easton, MD) equipped with an integrated sphere assembly over the range of 350 to 700 nm**.** The diffuse absorbance spectra obtained were converted by the Kubelka–Munk equation.

3. Photocatalytic Activity Evaluation with Mass Spectrometry

Photocatalytic activities of the samples were determined using the photodegradation of IPA under visible-light irradiation in a closed photoreactor. 0.05 g of photocatalyst powder was evenly dispersed in a thin film in an annular crystal tube [18]. Prior to the experiments, the sample was pre-treated at 150 °C for 30 min in dry N_2 (flowing at 100 mL min^{-1}), cooled to 30 °C, then exposed to O_2 flow (30 mL min^{-1}) for 60 min. Then, the inlet valve was closed and an appropriate amount of liquid IPA was injected into the reactor, producing the gaseous IPA concentration of 160 ppm. The photocatalytic reaction was carried out using a white daylight lamp (TOA, FL10D-EX, Taipei, Taiwan) after the samples were kept in the dark for 60 min to achieve gas-solid adsorption equilibrium. The main emission band is occurred at 545 nm and the

photon flux was measured as 0.131 W m^{-2}. The compositions of the gaseous products were monitored online with a quadrupole MS (SRS QMS300, Sunnyvale, CA) at regular intervals.

RESULTS AND DISCUSSION

1. Characterization of the Silver Vanadates

Table 1 indicates the crystal structure and specific surface area for the silver vanadates; the silver vanadates consisted of three types of phase: pure $Ag_4V_2O_7$ structure (JCPDS 77-0097) or pure α-Ag_3VO_4 structure (JCPDS 43-054) or mixed phases of $Ag_4V_2O_7$ and α-Ag_3VO_4. The HT4 samples had mixed phases of $Ag_4V_2O_7$ and α-Ag_3VO_4; as the hydrothermal time was increased to 6 h, HT6 had α-Ag_3VO_4 crystalline only. The $Ag_4V_2O_7$ crystalline was obtained for CTAB-SVO, indicating that the addition of CTAB might be favorable for the formation of $Ag_4V_2O_7$ crystal. Based on the XRD analyses, the structures of silver vanadates can be tuned by simply adjusting the hydrothermal time and adding the CTAB. The diffuse absorbance spectra of the as-prepared silver vanadates are shown in Fig. 1. The values of band gap for HT4 and HT6 samples were determined by the onset point of absorption curve and these values were found in the range of 2.3-2.4 eV; the value of the band gap for CTAB-SVO was found to be 2.5 eV, which is similar to the value reported by Konta et al. [8].

Table 1. Crystalline phases and surface areas of as-prepared silver vanadates

Sample	Crystal phase	BET surface area ($m^2 g^{-1}$)
HT6	α-Ag_3VO_4	1.7
HT4	α-Ag_3VO_4, $Ag_4V_2O_7$	2.0
CTAB-SVO	$Ag_4V_2O_{7W}$	6.5

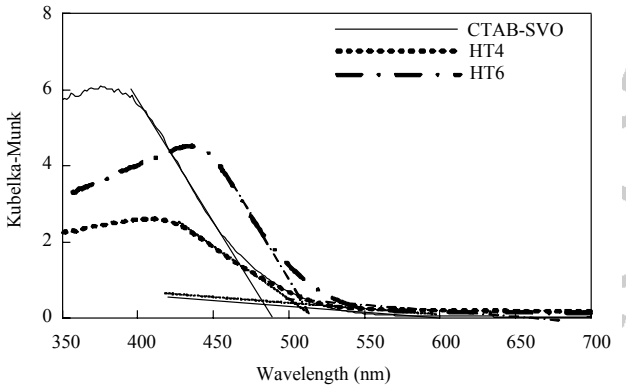

Fig. 1. Diffuse reflectance spectra of HT4, HT6 and CTAB-SVO.

2. Photocatalytic Activity and Role of Surface Hydroxyl Group

Figures 2 and 3 show the degradation kinetics of IPA vapor using various silver vanadates and P25 samples. During first 30 min of adsorption experiments, the concentrations of IPA vapor decreased rapidly due to the strong adsorption of IPA on catalyst surface. The degradation data of IPA in the early stage were fitted to a pseudo-first-order model. As shown in Fig. 3a, the photocatalytic degradation of IPA led to the formation of acetone and CO_2. After prolonged visible-light irradiation acetone was finally decomposed into CO_2 and H_2O. The decrease of the IPA concentration in the early stage is not sufficient for the comparison of photocatalytic activity; therefore, to evaluate the long-term photocatalytic activity of silver vanadates and P25, the amount of CO_2, a final decomposition product of gaseous IPA, was measured. The mineralization yield of gaseous IPA is defined as [6]:

$$\text{Mineralization (\%)} = \frac{1}{3}\frac{[CO_2]_{production}}{[CH_3CHOHCH_3]_{original}}100\%$$

For a 100% mineralization yield, it is expressed as 3 mol CO_2 mol^{-1} IPA. The results of the 1st-order apparent rate constant (k_{app}) and mineralization yield under visible-light illumination are listed in Table 2. For an irradiation time of 420 min, the mineralization yields of IPA were 35 and 11% for HT4 and P25, respectively. Based on the long-term increase of CO_2 concentration, the photocatalytic ability of the HT4 sample is significantly superior to that of P25.

As photodegradation of IPA may yield acetone (intermediate product) and CO_2 (final product), we monitored the adsorption of these three components to insight the conversion progress over the HT4. Figure 4 shows the spectrum of adsorption of IPA on HT4 samples in the dark for 60 min. The spectrum recorded upon the adsorption of IPA at room temperature has several peaks: 1383 and 1252 cm^{-1} peaks in the low wavenumber region are assigned to the δ(CH) mode of IPA; in the high wavenumber region, a very intense band at 2978 and a weak band at 2888 cm^{-1} were observed, corresponding to the stretching ν(CH) mode of methyl groups of IPA. The intensities of C-H stretching and C-H bending bands reached a steady level in the dark for 40 min.

The DRIFT spectra of adsorbed IPA, acetone and CO_2 on HT4 samples during 240 min of visible-light illumination are shown in Fig. 5. The IR spectra of HT4 samples equilibrated with IPA in the dark were taken as the initial state under illumination. After 60 min illumination, an obvious decline in the intensity of the band centered at 2978 cm^{-1} was observed for HT4 samples. Also, the band at 1670 cm^{-1}, due to stretching of the carbonyl group of adsorbed acetone, was observed after 60 min. Moreover, a strong peak

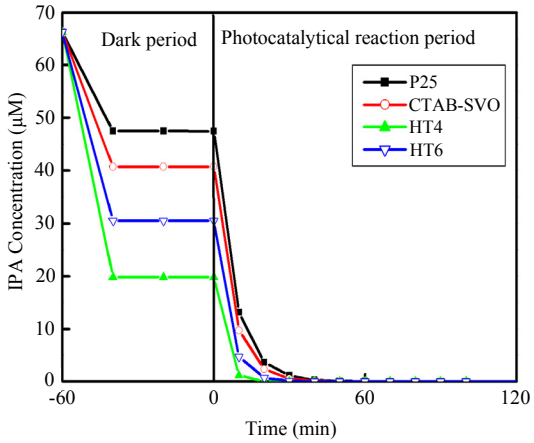

Fig. 2. Degradation curves of gaseous IPA decomposed by silver vanadates and by commercial TiO_2 (P25).

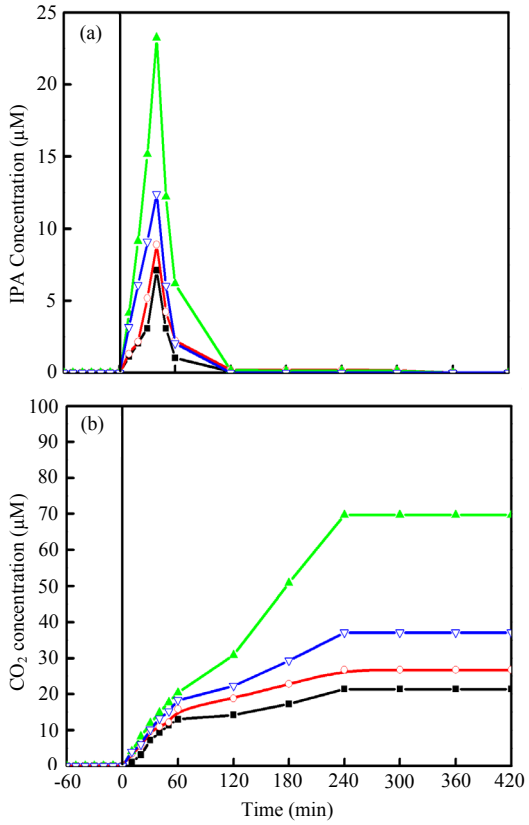

Fig. 3. Time-dependent concentrations for (a) acetone as main intermediate; (b) CO_2 as final product under visible light irradiation; (■) P25, (○) CTAB-SVO, (▲) HT4, and (▽) HT6.

centered at 2340 cm^{-1} is detected, corresponding to the antisymmetric stretch of the adsorbed CO_2 molecule. The antisymmetric stretch mode reached higher intensities after 120 min, indicating a high adsorption amount of CO_2 over HT4. Therefore it can be concluded that there were high adsorption amounts of acetone and CO_2 on HT4 samples between 60-120 min, resulting in the limited gaseous concentrations of these two products detected.

Table 2. Apparent rate constant and mineralization yield for various samples.

Sample	k_{app} (min^{-1})	Mineralization yield (%)
P25	0.13	11
HT4	0.28	35
HT6	0.19	19
CTAB-SVO	0.14	14

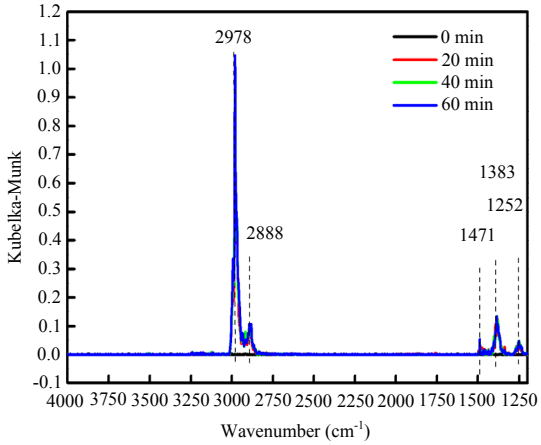

Fig. 4. DRIFT spectra of adsorbed IPA on HT4 samples during 60 min of darkness.

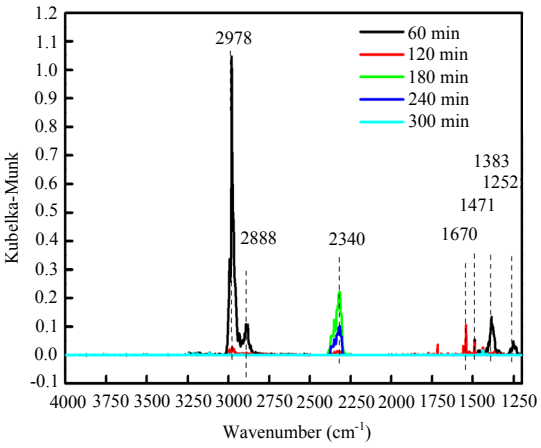

Fig. 5. DRIFT spectra of adsorbed IPA, acetone and CO_2 on HT4 samples during 240 min of visible-light illumination.

The photodegradation studies of IPA vapor indicate that the silver vanadates have a wide range of behavior, based on the k_{app} and mineralization data shown in Table 2. It is well known that either the adsorption process or the surface reaction is the rate-determining step for catalytic reactions; therefore, the photocatalytic reaction strongly depends on the crystalline structure, specific surface area and adsorption/desorption characteristics. For adsorption/desorption characteristics, the equilibrium adsorption amount of IPA in the dark de-

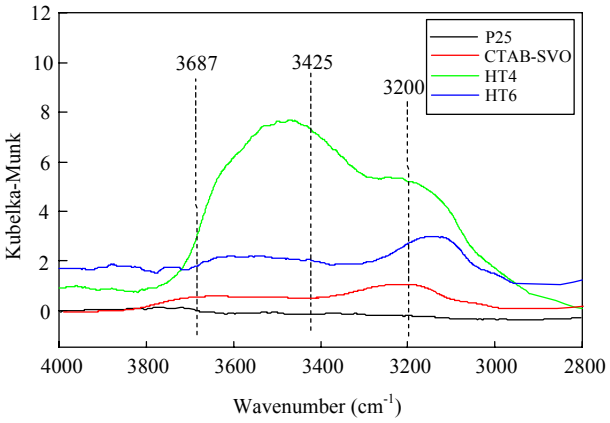

Fig. 6. Infrared spectra of OH groups on silver vanadates and P25 samples heated at 250 °C.

creased in the following sequence: HT4 > HT6 > CTAB-SVO > P25 (Fig. 2). In general, a higher surface area of the adsorbent would lead to higher adsorption capacity. Based on the data in Table 1, a large surface area of CTAB-SVO did not favor the adsorption of IPA. Therefore, the other parameter rather than surface area could play a leading role for the adsorption. The most important one is the surface chemistry of the adsorbents used. A literature survey indicates that the nature and distribution of surface OH groups can be the adsorption centers for reagents and/or products and are also the precursors of hydroxyl radicals responsible for many photodegradation processes [19-22]. To determine whether the surface hydroxyl groups of silver vanadates affect the adsorption of IPA and degradation abilities, in situ DRIFTS experiments were conducted. Figure 6 shows the FTIR spectra of the samples in the range 4000-2800 cm^{-1}. Within this range, two broad strong bands and one weak band corresponding to surface hydroxyl groups can be seen. For a quantitative comparison of OH groups, a deconvolution procedure was applied to the samples, which resulted in three Gaussian curves based on the IR assignments of OH groups (at 3200, 3425 and 3687 cm^{-1}) reported in the literature. The peak at 3200 cm^{-1} is the typical OH group chemically adsorbed on the surface of a photocatalyst [23]; the peaks at 3425 and 3687 cm^{-1} can be assigned to hydrogen bonded O–H stretching vibration [24] and linear ν(OH) [25], respectively. The amounts of various OH groups on the samples can be obtained by integrating the three individual curves, as shown in Table 3. In photocatalysis reactions, surface adsorbed water or the surface hydroxyl group acts as the trap for the photogenerated hole, preventing electron–hole recombination, forming oxidative hydroxyl radicals, and subsequently oxidizing the adsorbed molecules on the substrate surface. From Fig. 2 as well as Tables 2 and 3, it is evident that the high content of surface hydroxyl groups of HT4 results in the highest adsorption capacity for IPA and the highest apparent rate constant. With better α-Ag_3VO_4 crystallinity but a lower number of surface hydroxyl groups, HT6 had photocatalytic activity lower to that of HT4. The above experimental results confirm that the surface hydroxyl groups of as-prepared samples are a significant factor in photocatalytic activity.

Based on the aforementioned results of XRD and IR spectra of OH groups, the performance of photocatalytic activity of hydrothermal synthesis samples can be divided into three groups: HT4, HT6, and CTAB-SVO. As listed in Tables 1-2, HT4 consisted of mixed structures of $Ag_4V_2O_7$ and α-Ag_3VO_4, with α-Ag_3VO_4 as the major phase, and had higher photocatalytic activity than that of HT6, which had a stronger crystallinity of α-Ag_3VO_4 than that of HT4. In contrast, CTAB-SVO had pure $Ag_4V_2O_7$ and lower amount of surface hydroxyl groups than those of HT4 and HT6, resulting in the lowest photocatalytic activity. As indicated in Table 3, the amount of hydroxyl groups decreased in the following order: HT4 > HT6 > CTAB-SVO. From above explanations it can be deduced that crystal structure would be responsible for the amount of surface hydroxyl groups over silver vanadates.

CONCLUSIONS

The visible-light active silver vanadates photocatalysts were successfully synthesized using a direct and simple hydrothermal process. The Ag_3VO_4 powders, synthesized at the hydrothermal time of 4 h, were found to inherit the strongest absorption bands in visible light absorption, mixed structures of $Ag_4V_2O_7$ and α-Ag_3VO_4, with α-Ag_3VO_4 as the major phase,

Table 3. Calculated various OH peaks in the IR spectrum (region from 2800 to 4000 cm^{-1}) obtained for the samples at 250 °C

Sample	Isolated-OH			Total area
	OH group chemically adsorbed at 3200 cm^{-1}	H bonded O–H stretching vibration at 3425 cm^{-1}	ν(OH) linear at 3687 cm^{-1}	
P25	2.3	8.5	0.1	11
HT4	357	461	19	837
HT6	143	91	5.0	239
CTAB-SVO	55	5.8	2.9	63

and higher amount of surface hydroxyl groups, which leads to the highest photodegradation activity for IPA. The results indicated that hydrothermal-synthesis method is an appropriate method to prepare the novel visible-light active photocatalysts for environment and energy applications.

ACKNOWLEDGMENTS

The authors are grateful to the National Science Council of Taiwan, Republic of China, under Contract No. NSC 98-2221-E-168 -008 for supporting this study.

REFERENCES

1. Gebeyehu, D., C.J. Brabec and N.S. Sariciftci, Solid-state organic/inorganic hybrid solarcells based on conjugated polymers and dye-sensitized TiO_2 electrodes. Thin Solid Films, 403, 271-274 (2002).
2. Yamashita, H., M. Harada, J. Misaka, M. Takeuchi, K. Ikeue and M. Anpo, Degradation of propanol diluted in water under visible light irradiation using metal ion-implanted titanium dioxide photocatalysts. J. Photoch. Photobio. A, 148(1-3), 257-261 (2002).
3. Arana, J., A.P. Alonso, J.M.D. Rodrıguez, G. Colon, J.A. Navıo, J.P. Pena, FTIR study of photocatalytic degradation of 2-propanol in gas phase with different TiO_2 catalysts. Appl. Catal. B-Environ., 89(1-2), 204-213 (2009).
4. Huang, C.M., K.W. Cheng, Y.R. Jhan and T.W. Chung, Preparation of visible-light-active Ag and In-doped ZnS thin film photoelectrodes by reactive magnetron co-sputtering. Thin Solid Films, 515(20-21), 7935-7944 (2007).
5. Cheng, K.W., C.M. Huang, G.T. Pan, W.S. Chang, T.C. Lee and T.C.K. Yang, The physical properties and photoresponse of $AgIn_5S_8$ polycrystalline film electrodes fabricated by chemical bath deposition. J. Photoch. Photobio. A, 190(1), 77-87 (2007).
6. Huang, C.M., L.C. Chen, K.W. Cheng and G.T. Pan, Effect of nitrogen-plasma surface treatment to the enhancement of TiO_2 photocatalytic activity under visible light irradiation. J. Mol. Catal. A-Chem., 261(2), 218-224 (2007).
7. Kudo, A., Photocatalyst materials for water splitting. Catal. Surv. Asia, 7(1), 31-38 (2003).
8. Konta, R., H. Kato, H. Kobayoshi and A. Kudo, Photophysical properties and photocatalytic activities under visible light irradiation of silver vanadates. Phys. Chem. Chem. Phys., 5(14), 3061-3065 (2003).
9. Wang, J.S., S. Yin and T. Sato, Characterization and evaluation of fibrous $SrTiO_3$ prepared by hydrothermal process for the destruction of NO. J. Photochem. Photobiol. A, 187(1), 72-77 (2007).
10. Xie, H.D., D.Z. Shen, X.Q. Wang and G.Q. Shen, Microwave hydrothermal synthesis and visible-light photocatalytic activity of Bi_2WO_6 nanoplates. Mater. Chem. Phys., 103, 334-339 (2007).
11. An, T.C., J.K. Liu, G.Y. Li, S.Q. Zhang, H.J. Zhao, X.Y. Zeng, G.Y. Sheng, and J.M. Fu, Structural and photocatalytic degradation characteristics of hydrothermally treated mesoporous TiO_2. Appl. Catal. A-Gen., 350(2), 237-243 (2008).
12. Wei, Y.L. and P.C. Chang, Characteristics of nano zinc oxide synthesized under ultrasonic condition. J. Phys. Chem. Solids, 69(2-3), 688-692 (2008).
13. Zhang, A.P. and J.Z. Zhang, Characterization of visible-light-driven $BiVO_4$ photocatalysts synthesized via a surfactant-assisted hydrothermal method. Spectrochim. Acta A, 73(2), 336-341 (2009).
14. Chang, F.T., Y.C. Lin, H.L. Bai and B.S. Pei, Adsorption and Desorption Characteristics of the Semiconductor Volatile Organic Compounds on the Thermal Swing Honeycomb Zeolite Concentrator. J. Air Waste Manage., 53(11), 1384-1390 (2003).
15. Zhang, W.G., L.L. Zhang, Z.J. Jiang, R.Q. Li, X.J. Yang, X. Wang and L.D. Lu, Synthetic route to the nano-sized titania with high photocatalytic activity using a mixed structure-directing agent. Mater. Chem. Phys., 105(2-3), 414-418 (2007).
16. Shen, S.H., L. Zhao and L.J. Guo, Cetyltrimethylammoniumbromide (CTAB)-assisted hydrothermal synthesis of $ZnIn_2S_4$ as an efficient visible-light-driven photocatalyst for hydrogen production. Int. J. Hydrogen. Energ., 33(17), 4501-4510 (2008).
17. Huang, C.M., G.T. Pan, P.Y. Peng, and T.C.K. Yang, In-situ DRIFT study of photocatalytic degradation of gaseous isopropanol over $BiVO_4$ under indoor illumination. J. Mol. Catal. A-Chem., 327, 38-44 (2010).
18. Pan, G.T., C.M. Huang, L.C. Chen and W.T. Shiu, Immobilization of TiO_2 onto nonwoven fiber textile by silica sol: Photocatalytic activity and durability studies. J. Environ. Eng. Manage. 16(6), 413-420 (2006).
19. Chen, L.C., G.T. Pan, T.C.K. Yang, T.W. Chung, C.M. Huang, In situ DRIFT and kinetic studies of photocatalytic degradation gaseous benzene with

visible-light-driven silver vanadates. J. Hazard. Mater., 178, 644-651(2010).
20. Szczepankiewicz, S.H., A.J. Colussi and M.R. Hoffmann, Infrared spectra of photoinduced species on hydroxylated titania surfaces. J. Phys. Chem. B, 104(42), 9842-9850 (2000).
21. Marcì, G., M. Addamo, V. Augugliaro, S. Coluccia, E. García-López, V. Loddo, G. Martra, L. Palmisano and M. Schiavello, Photocatalytic oxidation of toluene on irradiated TiO_2: Comparison of degradation performance in humidified air, in water and in water containing a zwitterionic surfactant. J. Photochem. Photobiol. A, 160(1-2), 105-114 (2003).
22. Araña, J., C.G.I. Cabo, J.M. Doña-Rodríguez, O. Gonzá lez-Díaz, J.A. Herrera-Melián and J. Pérez-Peña, FTIR study of formic acid interaction with TiO_2 and TiO_2 doped with Pd and Cu in photocatalytic processes. Appl. Surf. Sci., 239(1), 60-71 (2004).
23. Janus, M. and A.W. Morawski, New method of improving photocatalytic activity of commercial Degussa P25 for azo dyes decomposition. Appl. Catal. B-Environ., 75(1-2), 118-123 (2007).
24. Colthup, N.B., L.H. Daly and S.E. Wiberley, Introduction to Infrared and Rama Spectroscopy. 3rd Ed., Academic Press, Boston, MA (1990).
25. Coronado, J.M., S. Kataoka, I. Tejedor-Tejedor and M.A. Anderson, Dynamic phenomena during the photocatalytic oxidation of ethanol and acetone over nanocrystalline TiO_2: Simultaneous FTIR analysis of gas and surface species. J. Catal., 219(1), 219-230 (2003).

Discussions of this paper may appear in the discussion section of a future issue. All discussions should be submitted to the Editor-in-Chief within six months of publication.

Manuscript Received: July 7, 2010
Revision Received: September 7, 2010
and Accepted: September 8, 2010